Biocatalysis and Agricultural Biotechnology 19 (2019) 101103

Contents lists available at ScienceDirect

Biocatalysis and Agricultural Biotechnology

journal homepage: www.elsevier.com/locate/bab

Fungal strain impacts the shape, bioactivity and multifunctional properties of green synthesized zinc oxide nanoparticles

Asem A. Mohamed[a], Amr Fouda[b], Mohamed Ali Abdel-Rahman[b,*], Saad El-Din Hassan[b], Mamdouh S. El-Gamal[b], Salem S. Salem[b], Tharwat I. Shaheen[a]

[a] National Research Centre, El-Behouth St., Dokki, P.O. 12622, Giza, Egypt
[b] Botany and Microbiology Department, Faculty of Science, Al-Azhar University, 11844, Nasr City, Cairo, Egypt

ARTICLE INFO

Keywords:
ZnO nanoparticles
Hexagonal NPs
Nanorod-NPs
Antibacterial textile
UV protection
NPs cytotoxicity

ABSTRACT

This work aimed to investigate the influence of fungal strains onto shape, functional properties, and potential applications of biosynthesized nanoparticles (NPs). The aqueous extract of two newly isolated fungal strains, *Fusarium keratoplasticum* strain (A1-3) and *Aspergillus niger* strain (G3-1), were used for synthesis of ZnO-NPs. Nanoparticles formation was confirmed by visual observation of color change and UV–visible spectroscopy. The morphological and structural properties of NPs were analyzed by Transmission Electron Microscope (TEM), Fourier Transform Infrared Spectroscopy (FT-IR), X-Ray Diffraction (XRD), Dynamic Light Scattering (DLS) and zeta potential analyses. Different ZnO-NPs shapes were obtained; where, *F. keratoplasticum* strain (A1-3) synthesized hexagonal NPs and *A. niger* strain (G3-1) synthesized nano-rod shape NPs. The antibacterial activities against Gram-negative and Gram-positive bacteria as well as *in vitro* cytotoxicity against three different animal cell lines exhibited that biocidal activity of NPs is a shape-dependent. Furthermore, nanoparticle shapes greatly affected the multifunctional properties of textile fabrics coated with ZnO-NPs. Nano-rod NPs showed enhanced antibacterial properties against pathogenic bacteria and UV-protection index compared to the hexagonal ZnO-NPs. Therefore, this work provides a gateway to explore shape-dependent properties of biologically synthesized NPs and their potentiality to be utilized for specific applications.

1. Introduction

Nanoparticles (NPs) have wide range of applications in chemical, pharmaceutical, medical and industrial purposes due to their size and morphology. NPs can be synthesized using various approaches. Physical and chemical synthesis approaches utilize harsh conditions of temperature, pressure, energy or hazard chemicals that lead to biological risks (Abdul et al., 2014). In contrast, biological synthesis approaches are becoming the most preferred methods as they are often green single step, cost effective, environment-friendly, clean, safe, and providing NPs of better defined sizes and morphology. In addition, biological systems act as capping agents to stabilize NPs (Fouda et al., 2017; Mohmed et al., 2017b; Ozin et al., 2009).

Among various NPs, metal oxides NPs have been widely investigated for their potential biomedical applications owing to their physicochemical properties. Of these, zinc oxide nanoparticles (ZnO-NPs) have gained much interest due to their excellent chemical and thermal stability even under harsh processing conditions. ZnO-NPs are utilized in various cutting-edge applications including sensors, cosmetics, environmental protection, biological and medicinal industries (Dagdeviren et al., 2013; Liu et al., 2009; Rasmussen et al., 2010).

NPs have demonstrated antimicrobial properties and therefore, recognized to be applied for reduction of infections, prevention of microbial colonization, elimination of microbes on the textile fabrics, or disinfection of various purposes (Hebeish et al., 2015). Beside it can be used as coating of implantable devices, bone cement, or dental materials (Wang et al., 2017). Moreover, NPs can be applied in textile industry and wound dressings to produce multifunctional fabric materials exhibiting antimicrobial activity, UV-blocking (Fouda et al., 2018), and self-cleaning (Bozzi et al., 2005).

However, the detailed antimicrobial mechanisms of metal oxide NPs have not been thoroughly explained, and even the same type of NP may exhibit adverse effects. Several factors have been reported to influence the action of NPs including size, shape, charge, zeta potential, surface morphology, crystal structure, specific surface area, surface energy, and atomic ligand deficiency (Pandurangan et al., 2016; Shaheen and El Aty, 2018). Of these factors, NPs shape affects the specific surface area

* Corresponding author.
E-mail address: mohamedali@kyudai.jp (M.A. Abdel-Rahman).

https://doi.org/10.1016/j.bcab.2019.101103
Received 20 January 2019; Received in revised form 7 March 2019; Accepted 18 March 2019
Available online 24 March 2019
1878-8181/ © 2019 Elsevier Ltd. All rights reserved.

and facet reactivity and, therefore, can cause varying degrees of cell damage (Wang et al., 2017). Therefore, bioactivities of NPs may be related to the change in shape and size due to electric field, phonons and plasmons surrounding the particles and hence change surface to volume ratio (El-Rafie et al., 2010). This change might exhibit a new feature in NPs physiochemical characteristic such as enhancement of chemical reactivity, increasing hardness and magnetic properties and enhancement of biological activity.

Previous studies investigated the characteristics of different shaped synthesized NPs. Roy et al. (2017) examined the effect of silver nanoparticle shapes (rod, flower shape, hexagonal and spherical) on adsorption capacity, electrochemical activity and photoluminescence sensing. Spherical shapes of nanoparticles exhibited easier fabrication whether *ex-situ* or *in-situ* fabrics (El-naggar et al., 2018; Fouda and Shaheen, 2017; Ganesan and Prabu, 2015; Hashem et al., 2017). Mahdi et al. (2017) biosynthesized nano-rod ZnO-NPs using *Xanthomonas campestris*, while Fouda et al. (2018) biosynthesized spherical ZnO-NPs by *Aspergillus terreus*. However, little concerns have been given to study the relation between microbial strain, biosynthesized NPs shapes and their bioactivity and multifunctional properties.

Therefore, this study aimed to report the influence of microbial biocatalyst on the shape of synthesized ZnO-NPs using zinc acetate as precursor. The structural properties of the green synthesized ZnO-NPs will be assessed. Comparing the characteristics, antimicrobial activities, and cytotoxic properties of different biosynthesized NPs will be analyzed. Furthermore, the multifunctional and the imparted properties of different-shaped ZnO-NPs will be examined on coated cotton fabrics.

2. Materials and methods

2.1. Fungal isolates

Two newly isolated fungal strains, *Fusarium keratoplasticum* strain (A1-3) and *Aspergillus niger* strain (G3-1) were isolated from soil samples and cultivated on potato dextrose agar medium. Those strains were identified based on cultural characteristics and morphological examination, as well molecular identification as previously described (Fouda et al., 2017; Mohmed et al., 2017a), and used for biosynthesis of ZnO-NPs. The ITS sequences which retrieved from this study, were deposited in Gene-Bank under accession numbers of MF479747 and ky465752 for *F. keratoplasticum* strain (A1-3) and *A. niger* strain (G3-1), respectively.

2.2. Biosynthesis of ZnO-NPs

2.2.1. Preparation of cell free filtrate

F. keratoplasticum strain (A1-3) and *A. niger* strain (G3-1) were grown in 100-mL malt extract broth medium in 250-mL Erlenmeyer flask and incubated at 28 ± 2 °C, 150 *rpm* for 5 days. Fungal biomasses were then filtrated using Whatman filter paper No. 1 and washed thrice with sterile distilled water to remove any media components. Fifteen gram of the harvested fungal biomass were re-suspended separately in 100-mL sterile distilled water and incubated at 28 ± 2 °C and 150 *rpm* for 48 h. Cell-free filtrates were then obtained by separating the fungal biomass by filtration using Whatman filter paper No. 1. The filtrates were centrifuged at 5000 *rpm* for 5 min to sediment any cell debris and then the supernatants (cell-free filtrates) were used for biosynthesis of ZnO-NPs.

2.2.2. Biosynthesis of ZnO-NPs using cell free filtrate

One hundred mL of each cell-free filtrate was mixed separately with zinc acetate [$Zn(CH_3CO_2)_2$] at final concentration of 2 mM and then incubated at 28 ± 2 °C, pH 10, 150 *rpm* for 24 h. A creamy-white formed precipitates of $Zn(OH)_2$ were collected and dried at 150 °C for 48 h to be used for further investigations.

2.3. Characterization of biosynthesized ZnO-NPs

2.3.1. Ultraviolet–visible (UV–vis) spectra

The formation of ZnO-NPs was monitored by visual assessment of solutions color changes. Biosynthesis of ZnO-NPs in a colloid solution was also monitored using UV–vis spectra as it exhibits an intense absorption peak due to surface plasmon excitation. Color changes in the cell-free filtrate/$Zn(CH_3CO_2)_2$ solutions were monitored using JENWAY 6305 Spectrophotometer at wavelengths of 200–800 nm. Cell free filtrate without $Zn(CH_3CO_2)_2$ was used as the blank.

2.3.2. Transmission electron microscopy (TEM)

Shape and size of the biosynthesized ZnO-NPs were determined using TEM. Specimens for TEM measurements were prepared using drop coating method by placing a drop of diluted colloidal solution containing ZnO-NPs on the copper grid coated by an amorphous carbon film and desiccating the solvent under vacuum for overnight before loading onto a specimen holder. AMT software was calibrated for NPs size measurements by digital TEM camera. The average diameter of the prepared ZnO-NPs was calculated from measuring over 100 nanoparticles in at least 10 random locations on the TEM grid in enlarged microphotographs.

2.3.3. Dynamic light scattering (DLS)

DLS was carried out using Zetasizer Nano instruments (Malvern Instruments, Worcestershire, UK) for characterization of NPs size in a solution. The samples were prepared by re-suspension of NPs in distilled water at 25 ppm, subjected to vortex to provide a homogeneous solution and transferred 1.5 ml to a square cuvette for measurements.

2.3.4. Fourier Transform-Infrared (FT-IR) spectroscopy

FT-IR analysis was used to determine the possible biomolecules existing in biosynthesized ZnO-NPs using JASCO FT-IR 4100 spectrometer. The samples (0.2 g) were mixed with potassium bromide (KBr) and loaded into discs at high pressure. IR spectra were scanned at a resolution of 4.0 cm^{-1} in the transmission mode of 400–4000 cm^{-1}.

2.3.5. X-ray diffraction (XRD) patterns of ZnO-NPs

XRD measurements of the ZnO-NPs were examined by X-ray diffractometer X'Pert Pro (Philips, Eindhoven, Netherlands) equipped with a proportional counter of Ni-filter Cu-K_λ radiation (δ = 1.5405 Å) and operated at a voltage of 40 kV and a current of 30 mA. The crystalline structure of ZnO-NPs was characterized in 2θ range of 10° to 80°.

2.4. Evaluation of bioactivity for biosynthesized ZnO-NPs

2.4.1. Antibacterial assay

Antibacterial activities of biosynthesized ZnO-NPs from the respective species were assessed using agar well diffusion method (Wang et al., 2009) to evaluate the minimum inhibitory concentration (MIC). Gram positive and Gram negative bacteria were used as test organisms namely *Bacillus subtilis* ATCC 6633, *Staphylococcus aureus* ATCC 6538, *Pseudomonas aeruginosa* ATCC 9027, and *Escherichia coli* ATCC 8739. Mueller–Hinton agar was prepared; each bacterial strain was swabbed uniformly onto the agar surfaces. Wells were cut out of agar plates using a standard cork borer (7 mm diameter). Stock solutions of each biosynthesized ZnO-NPs was prepared at different concentrations (1000, 500, 250, 125 ppm). 100 µL of these stocks were added into each agar well. Plates are kept in refrigerator for 1 h before incubation at 37 °C for 24 h. After incubation period, inhibition zones were measured in mm. Each treatment was performed in triplicates. Minimum ZnO-NPs concentration achieved complete growth inhibition was recorded as the MIC value.

2.4.2. Cytotoxicity assay

Different cell cultures of human colorectal adenocarcinoma cell line

(Caco-2), normal Vero (kidney of African green monkey) cell line and normal rat liver epithelial (colne-9) cell line were obtained through the American Type Culture Collection (ATCC). The *in vitro* cytotoxicity testing of ZnO-NPs was performed using cell viability assay MTT [3-(4, 5-dimethylthiazol-2-yl)-2, 5-diphenyl tetrazolium bromide]. Cells (1×10^5 cells/mL) were seeded in 96-well plates [0.2 ml medium/well] and incubated at 37 °C in 5% CO_2 incubator.

A stock solution of ZnO-NPs (1000 ppm) was prepared. After 24 h incubation, ZnO-NPs at varying concentrations (3.9, 7.81, 15.6, 31.2, 62.5, 125, 250, 500, and 1000 ppm) were added to the wells. The plates were then incubated for 24 h at 37 °C and 5% CO_2 incubator. After that, 30 µL of MTT (5 mg/mL in phosphate buffer saline) was added to each well and the plates were incubated at 37 °C in 5% CO_2 incubator for 1–5 h. After that, 1 ml of DMSO was added to each well and mixed well by micropipette. The color intensity of developed purple color due to formation of formazan crystals relate the presence of viable cells was visualized at 560 nm (Philip and Kundu, 2003). The experiments were performed in triplicates. Cell viability was calculated based on control (cells incubated without zinc oxide nanoparticles) as follows:

Cell viability (%) = (Absorbance of treatment/absorbance of control) × 100.

2.5. Application of ZnO-NPs for medical textiles

2.5.1. Load of ZnO-NPs onto cotton fabrics-based textiles

Cotton fabrics were firstly washed and dried before cutting into samples with sizes of 15 cm × 30 cm. Cotton fabrics were then padded with colloidal ZnO-NPs solution at certain safe concentration [based on MIC and *in-vitro* cytotoxicity results] and agitated for 5 min, then squeezed to 100% wet pick up with laboratory pad at constant pressure. Samples were dried at 80 °C for 5 min and then cured at 150 °C for 2 min. Various treatments were conducted as follow: Negative control of trypticasene soya broth [TSB] medium without bacterial inoculation; Positive control of untreated fabrics emerged in TSB inoculated by bacterial culture; blank, untreated fabrics emerged in TSB without inoculation; and fabrics treated with zinc oxide nanoparticle solutions.

2.5.2. Scanning electron microscopy (SEM) for cotton fabrics

The surface morphology and internal structure of treated cotton fabrics as compared to control was studied using SEM (JEOL, JSM-6360LA, Japan). Fabrics specimens were mounted on the specimen stabs and coated by the sputtering method to form thin film of gold. Energy Dispersive Spectroscopy (EDS) is related to SEM instrument and used to study the contents and distribution of NPs in fabrics sample.

2.5.3. Antibacterial activity of nanoparticles treated fabric

The antibacterial activity of different fabrics was evaluated against Gram positive bacteria [*Staphylococcus aureus* ATCC 6538, *Bacillus subtilis* ATCC 6633] and Gram negative bacteria [*Pseudomonas aeruginosa* ATCC 9027 and *Escherichia coli* ATCC 8739]. Squares of each fabric sample (1 cm) were prepared under aseptic condition and placed in 5 mL TSB inoculated with 100 µL of bacterial suspension (optical density at 630 nm = 1.0). The antibacterial efficiency was determined by comparing the reduction in $O.D._{630\ nm}$ of the treated samples with that of the positive control after 24 h. The reduction of bacteria (%) was calculated as follows:

$$R\ (\%) = [(A - B)/A] \times 100$$

where R, the reduction rate; A, optical density for positive control; and B, optical density for treated fabrics.

2.5.4. Ultraviolet protection factor (UPF) of fabrics

UPF is used to describe the ability of treated and untreated fabrics to block UV light. UPF value was evaluated in the range of 280–400 nm with difference of 10 nm using UV/Visible Spectrophotometer 3101 PC with a software version.

2.6. Statistical analysis

Data were statistically analyzed by sigma plot 12.5 program; means of three replications and standard error (SE) were calculated. One-way analyses of variance (ANOVA) test were used for multiple sample comparison, when normality and homogeneity of variance were satisfied.

3. Results and discussion

3.1. Biosynthesis of ZnO-NPs

Biological synthesis of nanoparticles and their oxides exhibits several advantages and consequently has acquired more attention as alternative to chemical and physical synthesis methods (Jiang et al., 2018). In this study, screening the ability of microbial biocatalyst to influence the shape of ZnO-NPs and the impact of the produced shapes on the imparted properties were investigated. Two newly isolated fungal species of *F. keratoplasticum* strain (A1-3) and *A. niger* strain (G3-1), were used for biosynthesis of ZnO-NPs using their metabolites contained in cell free filtrates. Firstly, white creamy precipitate of the hydrate ZnO ($ZnO{\cdot}H_2O$) was formed after drop-wise addition of NaOH to the mixture of fungal cell-free filtrate and zinc acetate under vigorous stirring. Secondly, this milky precipitate was collected by centrifugation prior calcination at 120 °C for 12 h in order to obtain high purity of biosynthesized zinc oxide NPs for characterization and further studies.

Fungal cell-free filtrates contain some metabolites such as enzymes and proteins which play a critical role in the synthesis of nanoparticles. The interaction between enzymes and/or proteins with metal salts results in the reduction of ions in case of metal nanoparticles or causes size reduction in metal oxide which mainly depends on the affinity of these moieties to stabilize the formed cluster at size below 100 nm (Fouda et al., 2018). Proteins may also able to further arrange and align the shape of the formed nanoparticles.

3.2. Characterization of biosynthesized zinc oxide NPs

3.2.1. UV–vis spectroscopy

Visual observation and strength of surface plasmon resonance (SPR) at different wavelength (200–800 nm) are the main criteria indicating the biosynthesis of ZnO-NPs. Our observation indicated color change of reaction mixture from colorless to turbid white. As shown in Fig. 1, the absorption spectra of ZnO-NPs synthesized by *F. keratoplasticum* strain (A1-3) and *A. niger* strain (G3-1) showed their maximum SPR bands at wavelength 390 nm. These results confirmed the formation of ZnO-NPs,

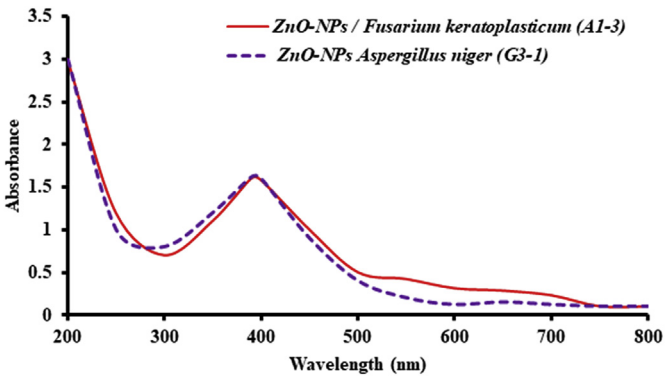

Fig. 1. UV–visible spectra of biologically synthesized ZnO-NPs by *Fusarium keratoplasticum* strain (A1-3) and *Aspergillus niger* strain (G3-1) at different wavelengths.

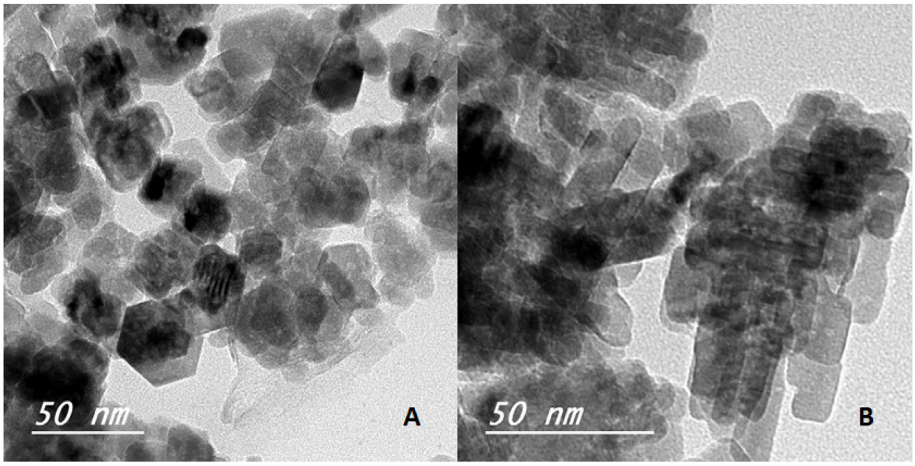

Fig. 2. TEM images for biologically synthesized ZnO-NPs. [A] Hexagonal shape synthesized by *Fusarium keratoplasticum* strain A1-3; [B] Nano-rod shape synthesized by *Aspergillus niger* strain G3-1.

where the characteristic SPR of ZnO-NPs is almost near of 370–400 nm (Vennila and Jesurani, 2017). The broad peaks observed for both samples at maximum SPR prolonging with the red shift of the wavelength might be pertaining to the shape of nanoparticles formed.

3.2.2. Transmission electron microscope (TEM)

Shape and size of biosynthesized ZnO-NPs were characterized using TEM as shown in Fig. 2. Hexagonal and nano-rod are two different shapes of ZnO-NPs which were successfully obtained from the bio-filtrate of *F. keratoplasticum* strain (A1-3) and *A. niger* strain (G3-1), respectively. The results showed that, the ability of the secreted fungal cell-free extract to cape and reduce size of the formed ZnO nanoparticles in a definite shape with main size average ranged from 10 to 42 nm and 8–38 nm for hexagonal and nanorod ZnO-NPs, respectively. These results suggest that, the shape of the fungal synthesized NPs is species-dependent. Recently, spherical ZnO-NPs with size of 10–45 nm have been produced using *Aspergillus terreus* AF-1 (Fouda et al., 2018). The challenge is to understand the behavior of proteins secreted by different biocatalysts in aligning and adjusting the particles in a definite shape such as rod, hexagonal, or spherical shapes; therefore, further investigation should be conducted.

3.2.3. Fourier Transform Infrared Spectroscopy (FT-IR)

FTIR measurements were carried out to identify the possible interaction between ZnO and protein molecules, which partially responsible for the synthesis, stabilization, and well dispersion of ZnO-NPs in the reaction mixture. FT-IR spectra were obtained from the purified white powdered ZnO-NPs (Fig. 3). The FT-IR spectra showed intense absorption peaks appeared at (3394.90, 2930.26, 1574.80, 1389.87, 1044.88 & 513.43 cm^{-1}) and (3436.50, 2936.80, 1605.54, 1340.85, 1024.38 & 515.59 cm^{-1}) by *F. keratoplasticum* strain (A1-3) and *A. niger* strain (G3-1), respectively. The broad peaks at 3394.90 and 3436.50 cm^{-1} are corresponding to O—H stretching group of phenols and alcohol due to the asymmetric stretch mode of amines N—H groups. Whilst, the existed peaks at 2930.26 and 2936.80 cm^{-1} are assigned to the stretching of methylene groups C—H of protein. The bands at 1574.80 and 1605.54 cm^{-1} were also attributed to the binding vibrations of amide I band of protein with N—H stretching band. Moreover, the bands observed at 1389.87, 1340.85, 1044.88, and 1024.38 cm^{-1} could be assigned to C—N stretching vibrations of aromatic and aliphatic amines. Finally, peaks lied at wavelengths 513.43 and 515.59 cm^{-1} refer to bending of alkene (=C—H) groups. Hence, the current study suggests that proteins or fungal bio-filtrate extracts bind readily to ZnO-NPs through either free amino or carboxyl groups of the proteins; moreover, the acquired shape of NPs changes according to the variation of protein binding with ZnO-NPs.

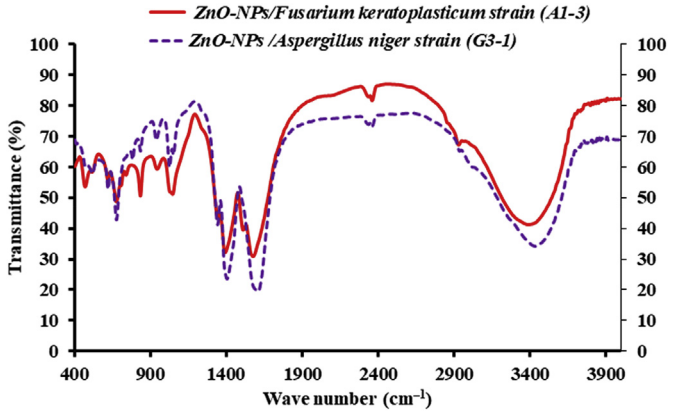

Fig. 3. FT-IR spectra of ZnO-NPs synthesized by *Fusarium keratoplasticum* strain A1-3 and *Aspergillus niger* strain G3-1.

3.2.4. X-ray diffraction (XRD) analysis

The crystalline nature of biosynthesized ZnO-NPs was confirmed using X-ray diffraction technique which agreed with those of the JCPDS data (89-7102 and 36-145 for hexagonal and nanorod ZnO-NPs, respectively). Data of XRD spectra revealed that diffraction peaks at 100, 002, 101, 102, 110, 103 and 112 detected at different 2θ values are corresponding to crystal plans of ZnO-NPs (Fig. 4). Interestingly, varied relative intensity of the diffraction peaks 100 to 002 revealing the different NPs shapes were existed regarding to whether fungal species was used. In the case of *F. keratoplasticum* strain (A1-3), the intensity between two peaks of 100 and 002 was similar (Fig. 4A), while in other case the intensity of peak 100 was greater than of peak 002. These results indicated that, the main shape of ZnO-NPs is hexagonal quartzite phase and their crystals tend to grow either horizontally in the case of *F. keratoplasticum* strain (A1-3) or in long ellipse shape to form rod nanoparticles in case of *A. niger* strain (G3-1) [Fig. 4B].

3.2.5. Dynamic light scattering (DLS) and zeta potential analyses

DLS is one of the most common techniques used for detection the distribution of particle sizes in a colloid solution based on intensity. The obtained ZnO-NPs were poly-dispersed mixture with average diameters of 163.34 nm (92.7%) and 135.5 nm (86.4%) for hexagonal and nanorod ZnO-NPs, respectively (Fig. 5). Also, Fouda et al. (2018) reported that DLS for spherical ZnO-NPs was 175.85 nm (95.4%). The obtained particle sizes measured by DLS was over expressed than those measured

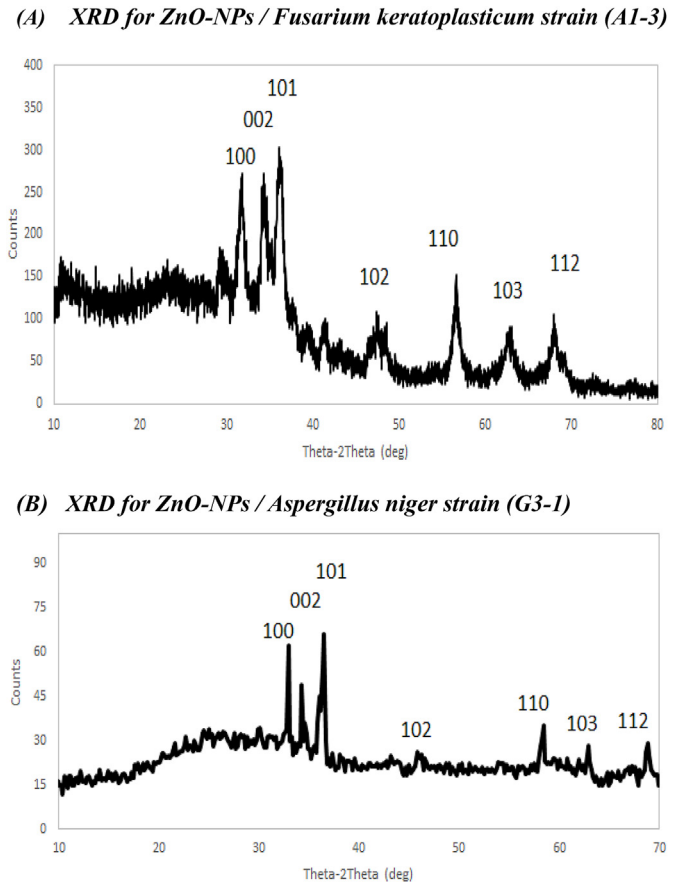

Fig. 4. XRD pattern of ZnO-NPs synthesized by: [A] *Fusarium keratoplasticum* strain A1-3, and [B] *Aspergillus niger* strain G3-1.

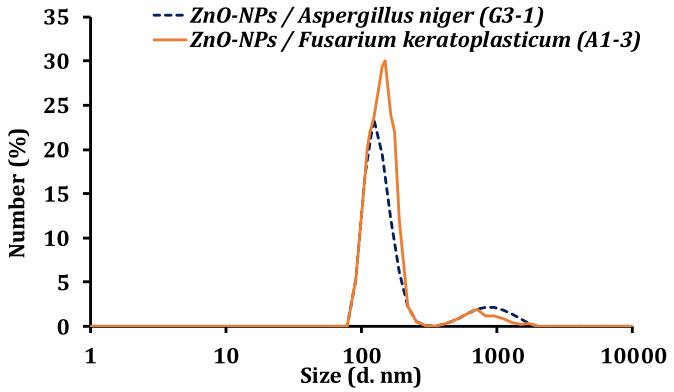

Fig. 5. Particle size distribution for ZnO-NPs synthesized by *Fusarium keratoplasticum* strain A1-3 and *Aspergillus niger* strain G3-1.

using TEM because the obtained size using DLS is not only related to metallic core of particles but also influenced by capping proteins and enzymes surrounding the particles (Aziz et al., 2014).

The acquired charge on the particles surface which measured by Zeta potential analyzer is responsible for colloidal solution stability and prevent the formation of aggregates with time. Zeta potential value for the obtained hexagonal and nanorod ZnO-NPs were −39 mV and −35 mV, respectively; which proven the stability of hydrodynamic solution. In general, high positive or negative zeta potential values (greater than +30 mV or smaller than −30 mV) makes the particles foreswear from each other without aggregation (Meléndrez et al., 2010).

3.3. Antibacterial assay of ZnO-NPs and MIC determination

To investigate the effect of different shapes of biosynthesized ZnO-NPs on their bioactivity, antibacterial activity was assessed against different pathogenic bacteria using agar well diffusion method as shown in Fig. 6 (A, B). The inhibition zones formed by ZnO-nanorod at 2000 ppm against Gram-positive bacteria were 23.6 ± 0.4 mm and 19.5 ± 0.2 mm for *Bacillus subtilis* ATCC 6633 and *Staphylococcus aureus* ATCC 6538, respectively. While that formed by ZnO-hexagonal shape were 22.0 ± 0.6 mm and 18.2 ± 0.7 mm, respectively. As well, the inhibition zones produced due to inhibitory effect of ZnO-NPs at 2000 ppm against *E. coli* ATCC 8739 and *Pseudomonas aeruginosa* ATCC 9027 (Gram negative bacteria) were 17.5 ± 0.3 mm and 16.1 ± 0.4 mm for nanorod shape, while in case of hexagonal shape, it was 15.7 ± 0.4 for both test organisms. The results indicated that nanorod ZnO-NPs have better inhibitory effects against Gram positive and Gram negative bacteria than those caused by hexagonal ZnO-NPs. These results confirmed that, the biological activity of NPs was influenced by their size and shape because different particle surfaces have variant thickness of surface atoms and electronic structures that lead to various chemical and physical properties (Khodashenas and Ghorbani, 2015). The inhibitory effect of ZnO-NPs might be related to suppression of enzymatic activities which emitted from the obstruction of DNA replication due to reaction of NPs with phosphorus moieties in DNA (Gupta et al., 2008), or due to the damage of cell membrane by inducing reactive oxygen species (ROS) production that lead to imbalanced redox state and oxidative stress (Manke et al., 2013).

The diameter of inhibition zones formed by green synthesized nanoparticles was dose dependent (Fouda et al., 2018; Hassan et al., 2018). Therefore, it is necessary to identify the lowest concentration that prevents bacterial growth (MIC) for the biosynthesized ZnO-NPs against each pathogen. To achieve this goal, different concentrations of ZnO-NPs were used (125–2000 ppm). Results represented in Fig. 6 evoked that, MIC for both rod and/or hexagonal ZnO-NPs were 250 ppm against Gram positive bacteria and 500 ppm against Gram negative bacteria. However, nanorod NPs is more effective than hexagonal NPs in bacterial inhibition even at low concentration of 250 ppm, suggesting as an evident the MIC is a shape-dependent.

3.4. Cytotoxicity assay

Cell viability is a main concern when nanoparticles are entered or contacted to cells. Therefore, we investigated the cytotoxicity of the two different shapes of biosynthesized ZnO-NPs (3.9–1000 ppm) by incubation with three different animal cell lines (Caco-2 as cancer cell line, Clone-9 and Vero cell lines as normal cells) using MTT assay. The IC50 estimated for the nanorod shape of ZnO-NPs were 127.2, 57.6 and 131.0 ppm, while IC50 for hexagonal ZnO-NPs were 20.1, 31.3 and 104.3 ppm for Vero, Clone-9 and Caco-2 cell lines, respectively (Fig. 7). The results of MTT assay showed that nanorod shape could be attributed to the stability of physicochemical properties of ZnO-NPs better than those found with hexagonal shape. In addition, the hexagonal ZnO-NPs exhibited higher toxicity toward carcinogenic cells (Caco-2) at low concentration than those caused by nanorod ZnO-NPs. It is expected that, the cell behavior will be varied in response to different shapes of NPs and is also based on the cell sort; however, the interesting finding of the current study is the cytotoxicity of nanoparticles is shape-dependent. Therefore, the present investigation indicated that the safe concentrations of biosynthesized ZnO-NPs for possible applications in concern to animal cells should be lower than 20.1 ppm in case of hexagonal shape and should be lower than 57.6 ppm in case of nanorod shape. The aforementioned results established undoubtedly that, the rod ZnO-NPs shape is more applicable safety at high concentrations in contrast to hexagonal shape of ZnO-NPs.

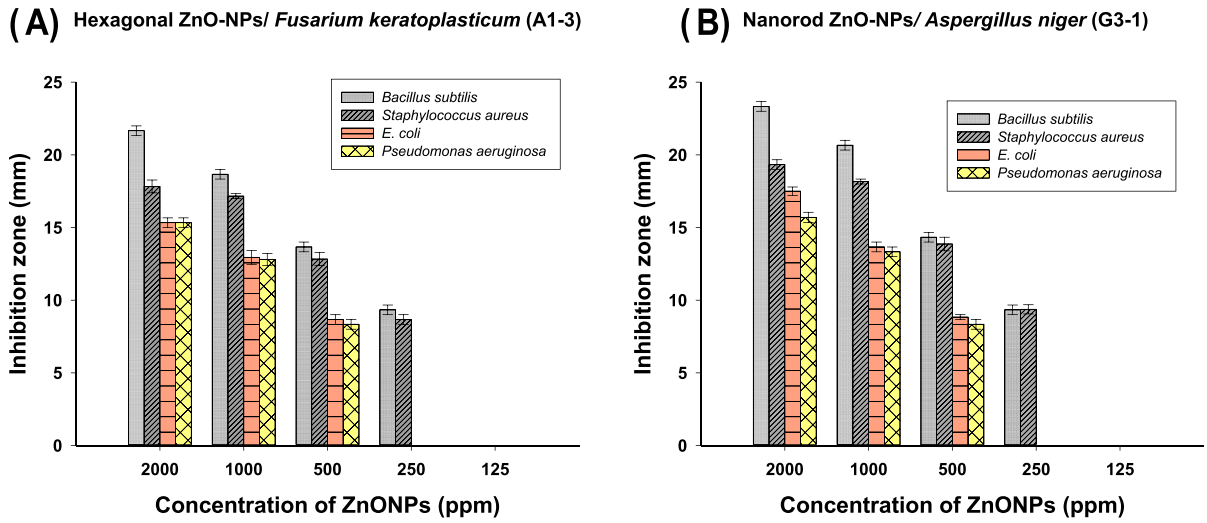

Fig. 6. Antibacterial activity against different pathogenic bacteria and MIC determination of: [A] Hexagonal ZnO-NPs synthesized by *Fusarium keratoplasticum* strain A1-3, and [B] Nano-rod ZnO-NPs synthesized by *Aspergillus niger* strain G3-1.

3.5. Application of hexagonal and nanorod ZnO-NPs in textile fabrics

Regarding to the unrivaled properties of ZnO-NPs in biomedical applications such as antibacterial and animal cell biosafety, the bio-synthesized hexagonal and nanorod ZnO-NPs were applied to produce multifunctional textile fabrics with improved properties against different pathogenic microbes. For this end, hexagonal and rods ZnO nanoparticles were re-suspended separately in dis. H_2O to obtain final concentrations of 20.0 and 57.0 ppm, respectively. SEM and EDX analysis were performed to detect the percent accumulation and chemicals composition of the two shape ZnO-NPs on cotton fabrics as shown in Fig. 8A–G. As clearly indicated from SEM images, the untreated cotton fabrics exhibited a very smooth surface (Fig. 8A) when compared with the surface of the treated cotton fabrics. This demonstrates the deposition of homogenously distributed hexagonal and nanorods ZnO-NPs on cotton surface as showed in Fig. 8B and 8E, respectively.

In addition, the chemical compositions of the treated cotton fabrics were determined through EDX analysis. As shown in mapping image (Fig. 8C and F), zinc element in hexagonal and nanorod ZnO-NPs represented 9.0% and 2.0%, respectively from the total number elements in the tested fabrics samples, whereas the weight percent of zinc in hexagonal and nanorod ZnO-NPs were 7.29 and 1.62%, respectively as showed in EDX spectra (Fig. 8D and G). Recently, zinc element in spherical ZnO-NPs treated cotton fabrics was occupied only 2.0% with weight percent of 1.03% (Fouda et al., 2018). Our results declared that, hexagonal ZnO-NPs was successfully deposited and intensively attached with the surface of treated cotton fabrics than ZnO-nanorods. This may be due to sharp-pointed ZnO-nanorods which lead to less deposit on the surface of treated cotton fabrics. These results also revealed that the potential properties of NPs of treated cotton fabrics are also NPs shape-dependent.

3.6. Effect of different shaped ZnO-NPs on textile fabrics properties

3.6.1. Antibacterial activity

The antibacterial activity of cotton fabrics loaded with different shapes of ZnO-NPs were assessed using microbial reduction percentage method as showed in Table 1. Our results revealed that, the antibacterial activity arisen from cotton fabrics coated with nanorod was higher than those obtained from hexagonal ZnO-NPs although the

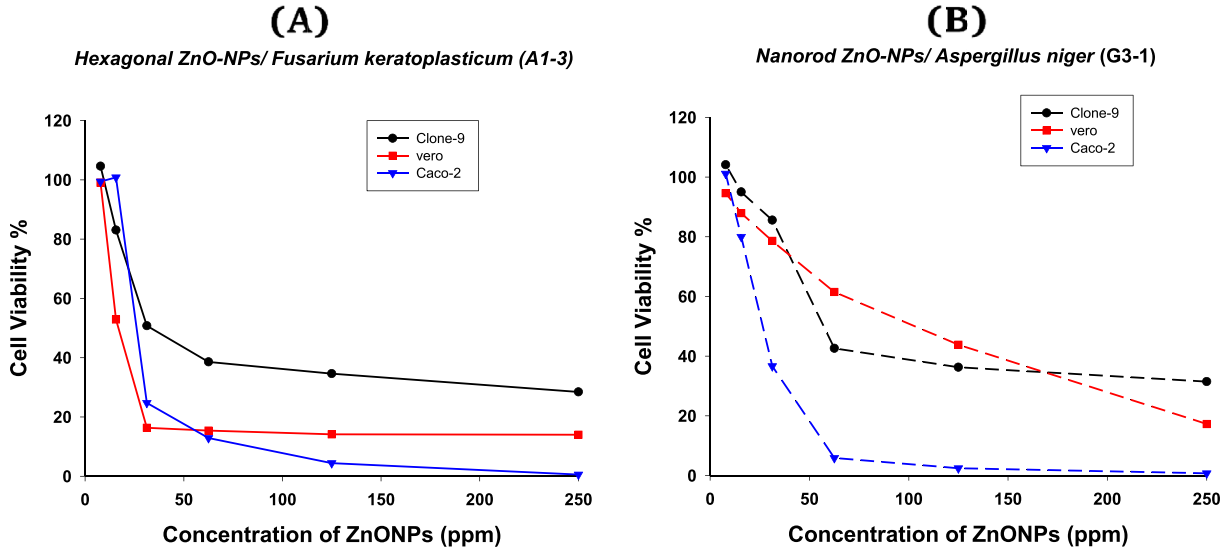

Fig. 7. Effect of ZnO-NPs on viability percent for Vero, Clone-9 and Caco-2 cell lines at different concentrations. [A] Effect of hexagonal ZnO-NPs, and [B] Effect of nano-rod ZnO-NPs.

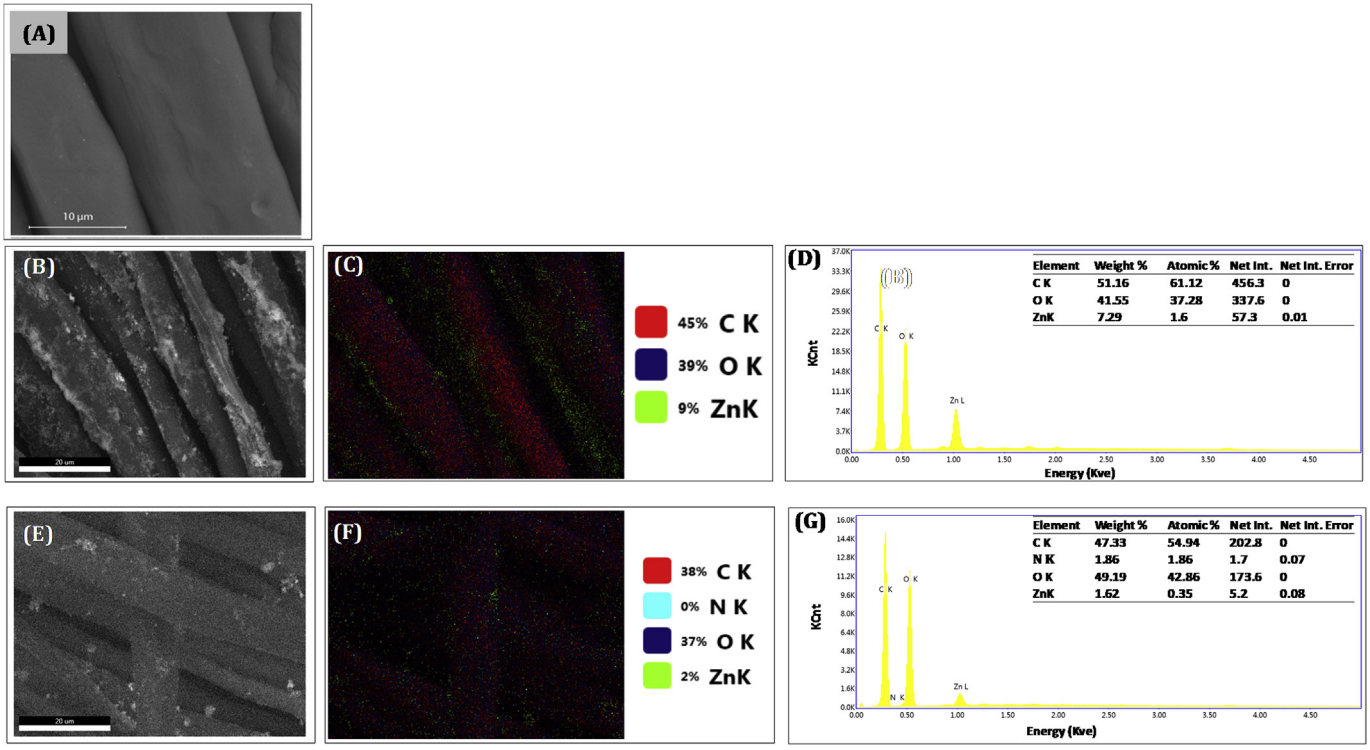

Fig. 8. SEM images of untreated cotton fabrics [A]; SEM image, mapping pictures of the surface, and EDX spectra with elemental analysis of cotton fabrics treated with hexagonal ZnO-NPs synthesized by *Fusarium keratoplasticum* strain A1-3 [B, C and D, respectively] and treated with nanorod ZnO-NPs synthesized by *Aspergillus niger* G3-1 [E, F, and G, respectively].

deposition ratio of nanorod on cotton fabrics was less than hexagonal. The reductions of bacterial viability of cotton fabrics loaded with hexagonal and nanorod ZnO-NPs were found in the range of 72.4–79.7% and 76.3%–84.3%, respectively (Table 1). The reduction of pathogenic bacterial viability was attained at 74.8–82.2% by cotton fabrics treated with spherical ZnO-NPs (Fouda et al., 2018). Our investigation is in contrast to the findings by Yamamoto et al. (1998) who reported that antibacterial activity of ZnO powder is mainly depended on the concentration and specific surface area of the powder irrespective of the shape and the crystallinity. Herein, we can conclude that antibacterial activity of the bio-synthesized ZnO-NPs is shape-dependent as have been confirmed previously by MIC test, and that might be attributed to differences in the structure even with the same type of NPs. Our results also manifested new behaviors regarding to the shape of biosynthesized ZnO-NPs used in the treatment of fabrics.

3.6.2. UV-protection

The ability of fabrics to UV-blocking is depend on several factors including quality of fiber, textile pattern, porosity, humidity, type of dyes and its concentration and existence of additives (Sricharussin et al., 2011). As ZnO-NPs loaded as additive onto the fabrics, we investigated the ability of different shape of ZnO-NPs coated fabrics on UV blocking. Table 2 showed the value of UPF, UVA and UVB for two shapes of ZnO-NPs coated cotton fabrics. The UPF protection values for treated cotton fabrics with hexagonal and nanorod ZnO-NPs were 25.5 and 29.1, respectively. These results indicated higher protection index as compared to the untreated cotton fabrics with UPF of 4.0 which is low protection index according to Australian/New Zealand Standard AS/NZS 4399:1996. Beside, Nanorod ZnO-NPs achieved higher protection index than obtained using hexagonal ZnO-NPs. Moreover, both shapes showed a higher protection index as compared to cotton fabrics treated by spherical ZnO-NPs having UPF value of 16.1 which is good protection index (Fouda et al., 2018).

UV is the invisible radiation radiated from sun and divided into two categories, UVA (315–400 nm) and UVB (290–315 nm). UVA and UVB have fatal effect on collagen fibers and cause skin ageing but UVB is more risky than UVA because of its direct impact on DNA and causes skin cancer (Dubrovski, 2010). Data in Table (2) showed that,

Table 2
Ultraviolet protection factor values of cotton fabrics untreated/treated with hexagonal and nanorod ZnO-NPs.

Fabrics	UPF protection value[a]	Blocking (%)	
		UVA	UVB
Untreated (control)	4.00	66.9	79.0
Treated with hexagonal ZnO-NPs.	25.5	83.2	90.3
Treated with nanorod ZnO-NPs.	29.1	88.3	94.2

[a] UPF; Ultraviolet protection factor.

Table 1
Bacterial viability of cotton fabrics treated by hexagonal and nanorod ZnO nanoparticles.

Samples	Viability reduction (%) of:			
	Staphylococcus aureus ATCC 6538	*Bacillus subtilis* ATCC 6633	*Pseudomonas aeruginosa* ATCC 9027	*Escherichia coli* ATCC 8739
Hexagonal ZnO-NPs coated cotton fabrics	77.5 ± 0.6	79.7 ± 0.5	72.4 ± 0.2	73.6 ± 0.4
Nanorod ZnO-NPs coated cotton fabrics	84.3 ± 0.3	84.3 ± 0.2	76.3 ± 0.3	76.8 ± 0.2

hexagonal ZnO-NPs loaded cotton fabrics can block UVA and UVB at 83.2% and 90.3%, respectively, while nanorods ZnO-NPs loaded cotton fabrics blocked UVA and UVB at 88.3% and 94.2%, respectively compared to untreated fabrics which block UVA and UVB at 66.9% and 79%, respectively. Our data indicated that cotton fabrics coated with rod ZnO-NPs was better than hexagonal and spherical shape in UV blocking. The retrieved UVA and UVB blocking values of the present study are also higher than those achieved by spherical ZnO-NPs coated cotton fabrics which blocked UVA and UVB at 76.3% and 85.4%, respectively (Fouda et al., 2018).

4. Conclusion

In this study, two newly isolated fungal strains, *Fusarium keratoplasticum* strain (A1-3) and *Aspergillus niger* strain (G3-1) were used for biosynthesis of ZnO-NPs. The differences in size, shape and structure of the biosynthesized NPs were evaluated using Transmission Electron Microscope, Fourier Transform-Infra Red spectroscopy, X-ray diffractometric and Dynamic light scattering analyses. The obvious difference was in shape, that proven to be hexagonal and nanorod for the NPs synthesized by *F. keratoplasticum* strain (A1-3) and *A. niger* strain (G3-1), respectively. Antibacterial activity against Gram-positive and Gram-negative bacteria, beside the *in vitro* cytotoxicity against animal cell lines indicated that the activity of NPs is a shape-dependent. Treatments of textile fabrics with safe dose of green synthesized ZnO-NPs exhibited potential activity against pathogenic bacteria and improved UV-protection as compared to untreated fabrics. Our results demonstrate the importance of fungal strain selection for production of specific NPs shape in respective to the properties and the possible applications of biosynthesized nanoparticles.

Conflicts of interest

Authors declare that there are no conflicts of interest.

Data availability

The data used to support the findings of this study are available from the corresponding author upon request.

Funding

This work was partially supported by a research grant from the Technology, Innovation, and Commercialization Office (TICO), Al-Azhar University, Cairo, Egypt.

Appendix A. Supplementary data

Supplementary data to this article can be found online at https://doi.org/10.1016/j.bcab.2019.101103.

References

Abdul, H., Sivaraj, R., Venckatesh, R., 2014. Green synthesis and characterization of zinc oxide nanoparticles from *Ocimum basilicum* L. var. *purpurascens* Benth.-lamiaceae leaf extract. Mater. Lett. 131.

Aziz, N., Fatma, T., Varma, A., Prasad, R., 2014. Biogenic synthesis of silver nanoparticles using *Scenedesmus abundans* and evaluation of their antibacterial activity. J. Nanopart. 2014, 6. https://doi.org/10.1155/2014/689419. Article ID 689419.

Bozzi, A., Yuranova, T., Guasaquillo, I., 2005. Self-cleaning of modified cotton textiles by TiO_2 at low temperatures under daylight irradiation. J. Photochem. Photobiol. A 174.

Dagdeviren, C., Hwang, S.W., Su, Y., Kim, S., Cheng, H., Gur, O., Haney, R., Omenetto, F.G., Huang, Y., Rogers, J.A., 2013. Transient, biocompatible electronics and energy harvesters based on ZnO. Small 9.

Dubrovski, P.D., 2010. Wowen Fabric and Ultraviolet Protection, Woven Fabric Engineering. InTech.

El-Naggar, M., Shaarawy, S., Hebeish, A.A., 2018. Multifunctional properties of cotton fabrics coated with *in situ* synthesis of zinc oxide nanoparticles capped with date seed extract. Carbohydr. Polym. 181, 307–316.

El-Rafie, M.H., Mohamed, A.A., Shaheen, T.I., Hebeish, A., 2010. Antimicrobial effect of silver nanoparticles produced by fungal process on cotton fabrics. Carbohydr. Polym. 80.

Fouda, A., Mohamed, A.A., Elgamal, M.S., Hassan, S.E., Salem, S.S., Shaheen, T.I., 2017. Facile approach towards medical textiles via myco-synthesis of silver nanoparticles. Der Pharma Chem. 9.

Fouda, A., Hassan, S., Salem, S.S., Shaheen, T.I., 2018. *In-vitro* cytotoxicity, antibacterial, and UV protection properties of the biosynthesized Zinc oxide nanoparticles for medical textile applications. Microb. Pathog. 125, 252–261.

Fouda, A., Shaheen, T.I., 2017. Silver nanoparticles: biosynthesis, characterization and application on cotton fabrics. Microbiol. Res. J. Int. 20, 14.

Ganesan, R.M., Prabu, H.G., 2015. Synthesis of gold nanoparticles using herbal *Acorus calamus* rhizome extract and coating on cotton fabric for antibacterial and UV blocking applications. Arab. J. Chem. 2015. https://doi.org/10.1016/j.arabjc.2014.12.017.

Gupta, P., Bajpai, M., Bajpai, S., 2008. Investigation of antibacterial properties of silver nanoparticle-loaded poly (acrylamide-co-itaconic acid)-grafted cotton fabric. J. Cotton Sci. 12, 280–286.

Hashem, M.M., El-Shafei, A.M., Sharaf, S.S., Abdel-Sattar, R., Mohamed, A.A., 2017. Development and evaluation of novel multifunction hybrid containing cationic softener/TiO_2/herbal oil for cotton based fabrics. Egypt. J. Chem. 2017, 171–183. https://doi.org/10.21608/EJCHEM.2018.2578.1204.

Hassan, S.E.L.D., Salem, S.S., Fouda, A., Awad, M.A., El-Gamal, M.S., Abdo, A.M., 2018. New approach for antimicrobial activity and bio-control of various pathogens by biosynthesized copper nanoparticles using endophytic actinomycetes. J. Radiat. Res. Appl. Sci. 11, 262–270.

Hebeish, A., Farag, S., Sharaf, S., Shaheen, T.I., 2015. Nanosized carbamoylethylated cellulose as novel precursor for preparation of metal nanoparticles. Fibers Polym. 16.

Jiang, J., Pi, J., Cai, J., 2018. The Advancing of Zinc Oxide Nanoparticles for Biomedical Applications. pp. 18.

Khodashenas, B., Ghorbani, H.R., 2015. Synthesis of silver nanoparticles with different shapes. Arab. J. Chem. https://doi.org/10.1016/j.arabjc.2014.12.014.

Liu, Y., He, L., Mustapha, A., Li, H., Hu, Z.Q., Lin, M., 2009. Antibacterial activities of zinc oxide nanoparticles against *Escherichia coli* O157:H7. J. Appl. Microbiol. 107.

Mahdi, Z.S., Rowshan, F.T., Nikzad, M., Zamani, S., 2017. Biosynthesis of zinc oxide nano-rods using *Xanthomonas campestris*. Biol. J. Microorg. 22.

Manke, A., Wang, L., Rojanasakul, Y., 2013. Mechanisms of nanoparticle-induced oxidative stress and toxicity. BioMed Res. Int. 2013, 15. https://doi.org/10.1155/2013/942916. Article ID 942916.

Meléndrez, M., Cárdenas, G., Arbiol, J., 2010. Synthesis and characterization of gallium colloidal nanoparticles. J. Colloid Interface Sci. 346.

Mohmed, A.A., Fouda, A., Elgamal, M.S., Hassan, S.E.-D., Shaheen, T.I., Salem, S.S., 2017a. Enhancing of cotton fabric antibacterial properties by silver nanoparticles synthesized by new Egyptian strain *Fusarium Keratoplasticum* A1-3. Egypt. J. Chem. 60.

Mohmed, A.A., Saad, D., Hassan, S., Fouda, A., Elgamal, S., Salah Salem, S., 2017b. Extracellular biosynthesis of silver nanoparticles using *Aspergillus* sp. and evaluation of their antibacterial and cytotoxicity. J. Appl. Life Sci. Int. 11 (2), 1–12.

Ozin, G.A., Arsenault, A.C., Cademartiri, L., 2009. Nanochemistry: A Chemical Approach to Nanomaterials. Royal Society of Chemistry, Cambridge.

Pandurangan, M., Enkhtaivan, G., Kim, D., 2016. Anticancer studies of synthesized ZnO nanoparticles against human cervical carcinoma cells. J. Photochem. Photobiol. B Biol. 158.

Philip, S., Kundu, G., 2003. Osteopontin induces nuclear factor κB-mediated promatrix metalloproteinase-2 activation through IκBα/IKK signaling pathways, and curcumin (diferulolylmethane) down-regulates these pathways. J. Biol. Chem. 278.

Rasmussen, J.W., Martinez, E., Louka, P., Wingett, D.G., 2010. Zinc oxide nanoparticles for selective destruction of tumor cells and potential for drug delivery applications. Expert Opin. Drug Deliv. 7.

Roy, E., Patra, S., Saha, S., Kumar, D., Madhuri, R., Sharma, P.K., 2017. Shape effect on the fabrication of imprinted nanoparticles: comparison between spherical-, rod-, hexagonal, and flower shaped nanoparticles. Chem. Eng. J. 321 (1), 195–206.

Shaheen, T.I., El Aty, A.A.A., 2018. *In-situ* green myco-synthesis of silver nanoparticles onto cotton fabrics for broad spectrum antimicrobial activity. Int. J. Biol. Macromol. 118, 2121–2130.

Sricharussin, W., Threepopnatkul, P., Neamjan, N., 2011. Effect of various shapes of zinc oxide nanoparticles on cotton fabric for UV-blocking and anti-bacterial properties. Fibers Polym. 12.

Vennila, S., Jesurani, S.S., 2017. Eco-friendly green synthesis and characterization of stable ZnO Nanoparticle using small Gooseberry fruits extracts. Int. J. ChemTech Res. 5.

Wang, L., Hu, C., Shao, L., 2017. The antimicrobial activity of nanoparticles: present situation and prospects for the future. Int. J. Nanomed. 12.

Wang, Y., Lu, Z., Wu, H., Lv, F., 2009. Study on the antibiotic activity of microcapsule curcumin against foodborne pathogens. Int. J. Food Microbiol. 136.

Yamamoto, O., Hotta, M., Sawai, J., Sasamoto, T., Kojima, H., 1998. Influence of powder characteristic of ZnO on antibacterial activity. J. Ceram. Soc. Jpn. 106 (1238), 1007–1011.